ELSEVIER

Journal of Nuclear Materials 278 (2000) 73–84

journal of nuclear materials

www.elsevier.nl/locate/jnucmat

Reaction sintered glass: a durable matrix for spinel-forming nuclear waste compositions

W.L. Gong[a,*], W. Lutze[b], R.C. Ewing[c]

[a] *Center for Radioactive Waste Management, The University of New Mexico, Albuquerque NM 87106, USA*
[b] *Department of Chemical and Nuclear Engineering, The University of New Mexico, Albuquerque NM 87131, USA*
[c] *Department of Nuclear Engineering and Radiological Sciences, University of Michigan, Ann Arbor, MI 48109, USA*

Received 5 June 1999; accepted 5 August 1999

Abstract

Glass formation by reaction sintering under isostatic pressure is an innovative process to vitrify refractory-rich high-level radioactive waste. We used a typical defense waste composition, containing spinel-forming components such as ~4 wt% of Cr_2O_3, ~23 wt% Al_2O_3, ~13 wt% Fe_2O_3, and ~9 wt% UO_2, with CeO_2 simulating UO_2. Reaction sintered silicate glasses with waste loading up to 45 wt% were prepared within three hours, by hot pressing at 800°C. The glass former was amorphous silica. Simulated waste was added as calcined oxides. The reaction sintered glass samples were characterized using scanning and analytical electron microscopy. The results show that extensive reaction sintering took place and a continuous glass phase formed. Waste components such as Na_2O, CaO, MnO_2, and Fe_2O_3, dissolved completely in the continuous glass phase. Cr_2O_3, Al_2O_3, and CeO_2 were only partially dissolved due to incomplete dissolution (Al_2O_3) or super-saturation and reprecipitation (Cr_2O_3 and CeO_2). The precipitation mechanism is related to a time dependent alkali content in the developing glass phase. Short-term corrosion tests in water showed that the glasses are chemically more durable than melted nuclear waste glasses. Based on hydration energies calculations, the long-term chemical durability of our reaction sintered glasses is expected to be comparable to that of rhyolitic and tektite glasses.

1. Introduction

Currently, vitrification by melting has been used exclusively to solidify high-level nuclear waste (HLW) [1]. The waste is mixed with glass forming additives or glass frit, melted and poured into steel canisters. A practically homogeneous melt must be produced to avoid settling of undissolved species in the melter. The melt is drained through a bottom outlet or an overflow spout. The final product is a relatively low melting borosilicate glass (1100–1150°C).

Certain types of defense high-level radioactive wastes, e.g., the tank wastes at Hanford, WA, USA [2], contain high concentrations of metal ions such as chromium, nickel, and iron, that form sparingly soluble spinel phases in the melter. The waste from the Hanford tank farm SX (Table 1) contains ~4 wt% Cr_2O_3, ~23 wt% Al_2O_3, and ~13 wt% Fe_2O_3. Experimental work conducted by Hrma et al. [3–7] showed that hematite (α-Fe_2O_3), corundum (α-Al_2O_3), and eskolaite (Cr_2O_3) form upon glass melting in addition to spinel. These phases usually have high liquidus temperatures, e.g., 1000–1200°C [4]. Eskolaite precipitated when the melt contained more than 0.13 wt% Cr_2O_3. The maximum waste loading for the SX-type waste was determined to be $\leqslant$13 wt% at 1150°C. The maximum waste loading for the A-type waste containing high spinel-forming components (e.g., ~60 wt% Fe_2O_3 and ~7 wt% MnO_2) was limited to be $\leqslant$17 wt% at 1150°C.

SX and other types of Hanford tank wastes require pretreatment, e.g., partial separation or blending with other wastes to avoid precipitation of crystalline phases in the melter and to maintain high waste loading, typically 30–40 wt%. Considering the large volumes of wastes to be treated (e.g., SX farm contains 1.69×10^4 m^3), pretreatment processes, generation of

* Corresponding author.

0022-3115/00/$ - see front matter
PII: S0022-3115(99)00226-3

secondary waste streams, increases in waste volume and processing time, additional space for storage and disposal will contribute significantly to the waste management costs. Therefore, alternative ways should be explored to make disposable forms for high-level radioactive waste. Vitrification by reaction sintering under pressure is one of them. We have applied this process successfully in the laboratory to vitrify zirconium-rich DST-type Hanford tank waste [8,9]. Advantages of this process are remarkable: lower processing temperatures ($\leqslant 850$°C versus 1150°C), less volatility of radionuclides, less equipment materials corrosion, no processing related waste loading constraints because phase separation does not affect the process. Waste loading is limited only by product quality, i.e., chemical durability of the glass. Potential disadvantages may include inhomogeneity of the glass, use of pressure, and mixing of powders.

Vitrification of HLW by sintering under pressure has been investigated previously [8–13]. A small pilot scale plant was operated in the early 1980s in Germany [11]. Terai et al. [10] investigated pressure sintering of simulated HLW with Pyrex glass frit. The chemical durability of their glass products was comparable to that of borosilicate glasses. At Centro Atomico Bariloche, Argentine, sintering of waste components with glass frits was performed by hot uniaxial pressing in cylindrical iron cans, 140 mm in diameter [12,13]. Fabrication of glass forms using hot uniaxial pressing and simulated light water reactor (LWR) and fast breeder reactor (FBR) waste, respectively, has been demonstrated in a small pilot plant at the Forschungszentrum Karlsruhe (KfK), Germany by making samples in cylindrical cans, 30 cm in diameter [11]. The highest waste loading was 35 wt%. The authors in references [10–13] used a glass frit with multiple components, e.g., borosilicate or aluminosilicate glass. Generally, only sintering was observed with almost no chemical reaction between waste components and the glass frit. Most waste phases were just encapsulated by glass particles.

Recently, we reported results on vitrification by reaction sintering under pressure [8,9]. We showed that substantial chemical reaction takes place with the waste phases when the glass frit is replaced by amorphous silica. A simulated Hanford tank waste with 30 wt% ZrO_2 (DST-type waste) was vitrified and yielded a homogenous glass with clusters of nano-sized zirconia crystallites precipitated from a supersaturated glass phase. The waste loading ranged between 30 and 50 wt%. The present study focuses on the vitrification of spinel forming wastes. The chromium-rich SX waste was selected for this work. Based on the work with DST-type waste, we intend to show that the types of wastes causing problems upon glass melting can be readily vitrified by reaction sintering under pressure. Glass formation by reaction sintering could then be proposed as a new and versatile technology to vitrify radioactive waste and to fabricate glass and glass–ceramics for other applications [14].

2. Experimental

2.1. Preparation of simulated SX-type waste

The estimated SX-type waste composition [2] and the simulate are given in Table 1. Cr, Mn, Ce, Fe, and Al were introduced as crystalline oxides: Cr_2O_3, MnO_2, CeO_2, Fe_2O_3, and Al_2O_3. Ca and Na were introduced as $Ca(OH)_2$ and sodium oxalate ($Na_2C_2O_4$), respectively. Fission products were deleted. Their concentration is relatively small in the SX-type waste. It can be expected that the behavior upon sintering of Cs and Sr, the main radionuclides in the waste, is similar to that of Na and Ca, respectively. Uranium ($\sim$9 wt% in the waste) was simulated by CeO_2. Both CeO_2 and UO_2 are of the fluorite structure-type. Their ionic radii are close, 0.097 nm (Ce^{4+}) and 0.100 nm (U^{4+}), coordination number 8, indicating that the crystal chemical behavior is similar. The only difference is that Ce^{4+} is more easily reduced to Ce^{3+} than U^{4+} to U^{3+}. Commercially available, fused amorphous silica powder (<325 mesh) was added as the glass former. All constituents were ball-milled using acetone as a mixing and milling medium. After 8 h of milling, the product was dried in air.

Milled powder mixtures were characterized by measuring particle size distributions in a Coulter® LS Particle Size Analyzer. In terms of number statistics, the mean particle size of the glass precursor materials was about 0.6 μm. In terms of volumetric statistics, the mean size is 5 μm, ranging from 1 to 20 μm. Fig. 1 shows the particle size distribution.

The powders were heated in air at 320–550°C until sodium oxalate was completely decomposed, as deter-

Table 1
Composition of actual and simulated TF–SX waste

Oxide	TF–SX	Simulated TF–SX
SiO_2	9.37	9.44
Na_2O	33.93	35.78
CaO	1.24	1.34
Fe_2O_3	12.76	12.85
Al_2O_3	22.74	22.90
Cr_2O_3	3.92	3.95
MnO_2	1.67	2.21
CeO_2	2.07	11.35
Others[a]	12.26	–
Total	100.00	100.00

[a] Others include NiO 0.30, SO_3 0.22, U_3O_8 9.19, and balance 2.09 (wt%). CeO_2 is used to simulate uranium oxide; MnO_2 represents MnO_2, NiO, and PbO_2; Na_2O represents Na_2O, K_2O, and Cs_2O.

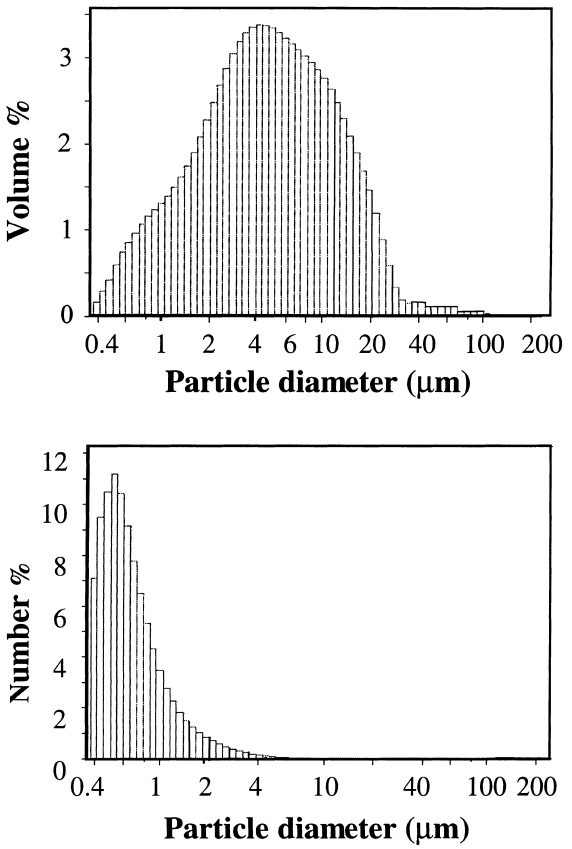

Fig. 1. Particle size of powder precursor (35 wt% of SX-type waste simulate mixed with amorphous silica).

mined by weight loss measurement. Stirring the mixture during heating ensured that Fe_2O_3 and CeO_2 were not reduced. To destroy particle agglomerates, the mixture was milled again.

2.2. Pressing

Powders were compacted at room temperature in a cylindrical die of 1.125 in. diameter. A pressure of 80 MPa was applied for two hours to shape and densify the green product. Pellets weighed 12 g. These samples were placed in an oven inside the pressure vessel of a hot isostatic press. Hot pressing was performed in a MINI-HIP'Per model SL-1 by heating the pellets to 800°C at 7 MPa. Argon was used as the pressurizing gas. The heating rate was 27°C/min. The holding time was 1 h at this setpoint. The low gas pressure was applied to reduce penetration of the gas into the samples during the early stage of reaction sintering. The pressure was then raised to 28 MPa. The holding time was 2 h at 800°C and at this pressure to complete the solid state reaction sintering process. The samples were cooled at a rate of 27°C/min. Reaction sintered glasses were produced with waste loading of 30, 35, 40, and 45 wt%. These samples were designated SG/30SX, SG/35SX, SG/40SX and SG/45SX, respectively.

2.3. Solid state analysis

The reaction-sintered glasses were characterized in terms of chemical composition and microstructure using energy dispersive X-ray spectroscopy (EDS), scanning and transmission electron microscopy (SEM and TEM). SEM was performed on polished samples using a JEOL 8000lv SEM operated at 20 keV. The SEM was equipped with an Oxford Link ISIS EDS system. A digitized camera was used to record secondary and backscattering electron images. Analytical electron microscopy (AEM) was performed with sintered glass samples using a JEM 2000FX electron microscope with a Noran TN-5500 EDS system and a JEM 2010 with an Oxford Link ISIS EDS system. The microscopes were operated at 200 keV. Specimens for the AEM study were made by sputtering (4 keV Ar ions) from mechanically polished thin sections (30 μm in thickness). Most of the EDS analyses were obtained using an Oxford Link ISIS EDS system attached to the JEM 2010 microscope. Some of the EDS analyses were also performed with a Noran TN-5500 EDS system attached to the JEM 2000FX. The K-factors used in all the calculations were calibrated in the laboratory. Final results were calculated and normalized to 100 wt%, based on the stoichiometry of oxides. Oxygen was not measured. The analytical errors for major elements were ±5% and ±20% for minor elements.

2.4. Chemical durability tests

The sintered glass samples were cut into rectangular shape using an oil-lubricated low-speed diamond saw. The samples were polished with 1–30 μm diamond lapping disks. The final polishing was made using 0.05 μm colloidal silica. Corrosion tests were carried out following the MCC-1P procedure described in Ref. [15]. Experimental Details for corrosion tests were reported in Ref. [9]. The sample surface area to solution volume ratio (S/V) was 10 m^{-1}. Leaching tests were run for 1, 3, 7, 14, or 28 days at 90°C. After cooling to room temperature an aliquot of the leachate was taken to measure the pH. Then, 10 ml of the remaining solution were used for chemical analysis.

To measure Na, 1 ml of the leachate was mixed with 2 ml of 6 N HCl containing 5 g/l Cs^+ in a 10 ml volumetric flask. Water was added to reach a total volume of 10 ml. Na was measured using absorption flame spectrometry with a detection limit of 0.5 mg/l. Si was also measured by absorption flame spectrometry. The normalized mass loss of the ith element $(NL)_i$ in g/m^2, was calculated using the equation $(NL)_i = C_i/(f_i \cdot S/V)$ where

C_i is the concentration in the leachate in g/m^3, and f_i is the mass fraction of the ith element in the glass.

3. Results

3.1. Microstructure

Fig. 2 is a SEM micrograph of a sintered glass sample with 40 wt% SX-type waste. Fig. 3 shows the same sample at a higher magnification. The microstructure of samples with different waste loading (30, 35, and 45 wt%) is similar to what is shown in Figs. 2 and 3. The gray background is the glass phase. Within the glass phase is a second glass phase, visible as round or irregularly shaped dark gray areas. The white and gray spots are crystals of different composition. The white particles in the glass matrix are CeO_2 and Cr_2O_3. The gray particles with a prismatic habit are Al_2O_3. The volume fraction of the crystals increases with increasing waste loading. Pores are visible with diameters less than a few microns (dark, round spots). There are some pores with diameters of 50 μm and higher. The porosity was estimated to range between 1 and 3 vol% for all samples. The microstructure is similar to that observed with glasses that contained a ZrO_2-rich (DST-type) Hanford tank waste [8,9].

Fig. 3 shows the same sample as Fig. 2 but at a higher magnification. The dark areas constituting the second glass phase are shrinking cores of what were originally amorphous silica particles. Their size decreases with increasing sintering time. Higher Z elements have lower concentrations near the center of these cores and give rise to brighter contrast toward the surface where they are enriched. We did not attempt to make reaction-sintered materials with only one glass phase. This would be necessary if the second glass phase had a deleterious effect on glass properties such as chemical durability. The glass samples described in this study are already chemically more durable than a commercial reference nuclear waste glasses (see below).

Fig. 4 shows individual prismatic Al_2O_3 particles. They were identified as euhedral corundum. The long

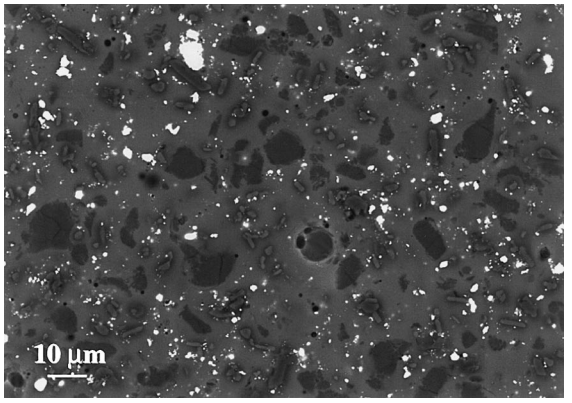

Fig. 2. SEM micrograph of glass sample SG/40SX. Gray background is the glass phase; darker large areas (10–15 μm) constitute second glass phase. Bright contrast: crystals of ceria (CeO_2); gray contrast: corundum (Al_2O_3) crystals; small round spots are pores.

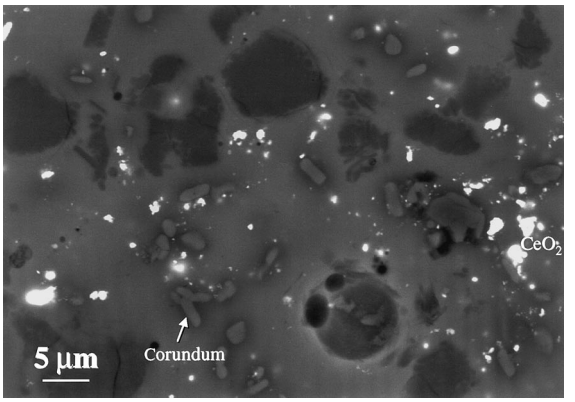

Fig. 3. SEM micrograph of sample SG/40SX at larger magnification. Same features as in Fig. 2. Second glass phase constitutes shrinking cores within the continuous glass phase.

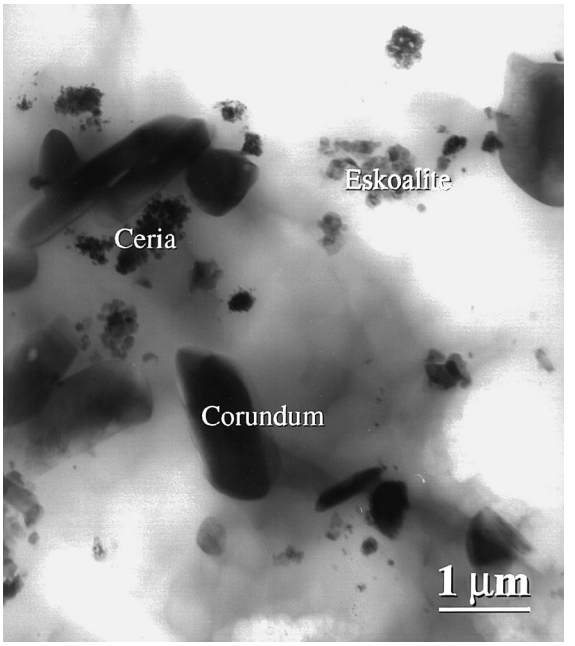

Fig. 4. TEM bright field image of glass phase (lighter shades of gray) with clusters of ceria (CeO_2) and eskoalite (Cr_2O_3) crystals and individual crystals of corundum (Al_2O_3) in the glass matrix (glass sample SG/35SX).

axis of the corundum crystals ranges from 1 to 5 μm. Chromium was found in the form of eskolaite (Cr_2O_3) forming clusters and so did ceria (CeO_2). All three phases are embedded in a glass phases (lighter shades of gray).

Fig. 5 shows ceria as nano-size (~50 nm) crystals. The inset of the micrograph is an electron diffraction pattern identifying cubic CeO_2 with fluorite-type structure. Individual crystals are a factor of 20–100 smaller than the ones in the starting material. As seen, the nano-size crystals form larger clusters.

As the concentration of CeO_2 increases in the sample (higher waste loading), the clusters grow, the number density of individual crystals increases (Fig. 6), and individual crystals begin to share grain boundaries (Fig. 7) and grow together.

Fig. 8 shows that eskolaite crystallites are larger (0.1–0.3 μm) than ceria crystals. Although eskolaite and ceria

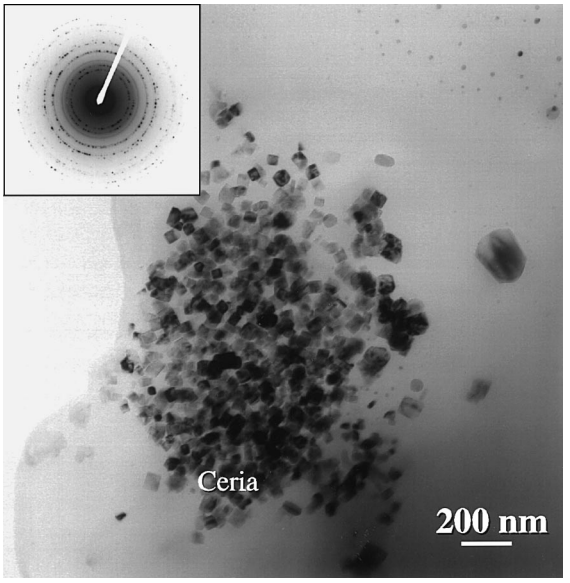

Fig. 5. TEM bright field image showing a cluster of euhedral, cubic ceria crystallites (40–80 nm in size) in the glass phase of sample SG/35SX. The inset is the electron diffraction pattern of ceria.

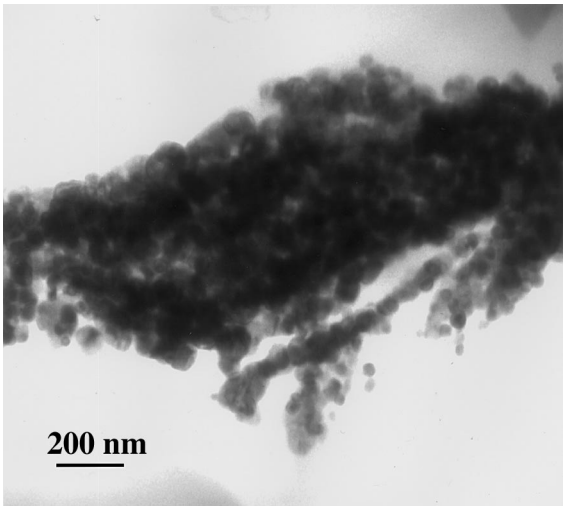

Fig. 6. TEM bright field image showing a cluster of ceria crystallites within the glass phase of sample SG/45SX. Small crystals seen in Fig. 5 grow together at higher Ce concentration, i.e., higher waste loading.

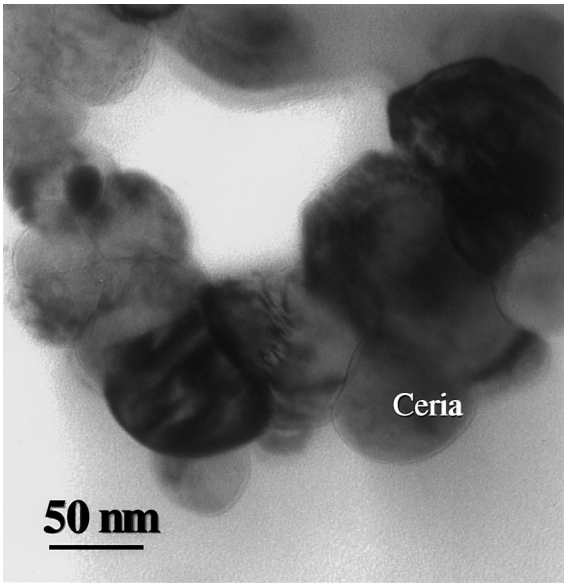

Fig. 7. TEM bright field image of glass sample SG/45SX showing the ceria cluster in Fig. 6 with grain boundaries in contact.

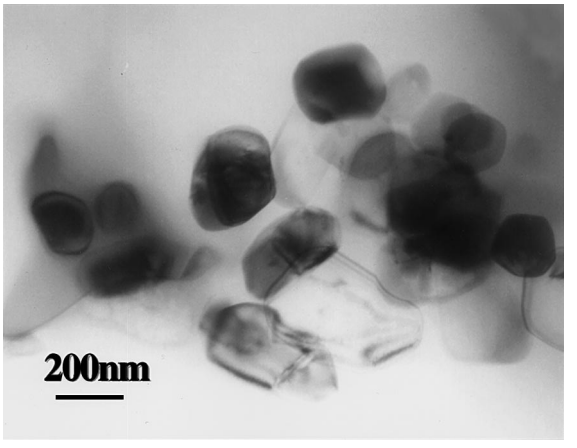

Fig. 8. TEM bright field image showing euhedral eskolaite crystals in the glass phase of sample SG/35SX.

Table 2
Compositions of reaction sintered glasses

Sintered glasses Number of analyses	SG/30SX 18	SG/35SX 13	SG/40SX 14	SG/45SX 14
SiO_2	74.67	70.68	69.71	68.65
Na_2O	12.83	13.66	14.61	15.64
CaO	0.87	0.85	0.96	0.93
Fe_2O_3	5.29	6.54	6.79	6.35
Al_2O_3	2.75	3.45	2.85	4.33
Cr_2O_3	0.24	0.65	0.69	0.79
MnO_2	0.91	1.15	1.02	0.90
CeO_2	2.43	3.02	3.34	2.41

crystallites differ in size, their size distributions are narrow, compared with that of the starting materials. As with ZrO_2 particles [9], the almost uniform size of ceria and eskolaite crystals suggests that these particles are formed by precipitation rather than incomplete dissolution. Note that clusters of ceria and eskolaite crystallites occur mostly in places that constituted phase boundaries in the powder mixture prior to sintering. Corundum crystals do not share the feature of the other crystal phases.

3.2. Composition of the glass matrix phase

Compositions of the glass matrix phase are shown in Table 2. All waste constituents dissolved in the glass matrix phase. Na_2O, CaO, MnO_2, and Fe_2O_3 dissolved completely; Al_2O_3 (≈45 wt%), CeO_2 (≈75 wt%) and Cr_2O_3 (≈50 wt%) dissolved only partially. The rest was found as corundum, ceria and eskolaite crystals embedded in the glass phase as shown in the previous section. The solubility of the partially dissolved oxides did not change significantly with increasing waste loading.

3.3. Chemical durability

The results of short-term chemical durability tests are given in Table 3. Fig. 9 shows the normalized mass loss of silicon over 7 days for the glasses SG/35SX, SG/40SX, and SG/45SX. All data are for 90°C in deionized water. The slopes of the curves are proportional to the reaction rate of each glass. The rates for the sintered glasses are compared with that of a French R7T7-type glass for commercial HLW [1]. The data for SG/30SX yield the same curve as for R7T7 glass and, therefore, are not shown in Fig. 9. The applied experimental conditions allow us to measure the glass network dissolution reaction for a short period of time, essentially as long as changes in the water composition are negligible. The glass network dissolution rate in water is a materials property depending only on glass composition, temperature and pH. At constant pH and temperature, the dissolution rate is a zero order chemical reaction and a straight line with a positive slope of one is expected when plotting log concentration of silicon as a function of log time. Usually, concentration is converted to mass of glass dissolved per unit area, the normalized mass loss NL. The data from Fig. 9 were plotted on log-scales as shown in Fig. 10. Straight lines with a slope of one are obtained, indicating that we measured the time independent dissolution rate of the glass network. The rate, $d(NL_{Si})/dt$, decreases with increasing waste loading between 30 and 45 wt%. The highest rate, 1.0 g/m^2/d, was measured for SG/30SX, the lowest, 0.1 g/m^2/d, for SG/45SX.

Results in Table 3 show an increase in pH in all leachates, suggesting that there was ion exchange between Na^+ in the glass and H^+ in solution. However,

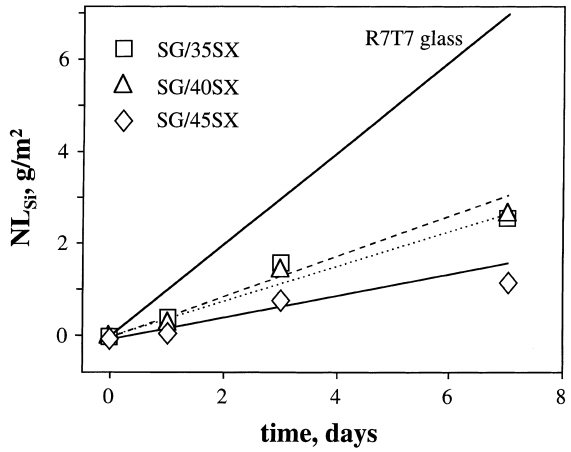

Fig. 9. Results of 7-day chemical durability tests (90°C, DI water). The normalized mass loss of Si is plotted as a function of time for glass samples SG/35SX, SG/40SX, and SG/45SX, and a French R7T7-type LWR waste glass. The slopes of the curves are the glass matrix dissolution rates (data for SG/30SX are not shown because they yield the same curve as for R7T7).

Table 3
Normalized mass losses of Na and Si (MCC-1, 90°C)

Sinter glasses	Time (days)	NL_{Na} (g/m^2)	NL_{Si} (g/m^2)	Final pH
SG/30SX	1	5.6	3.5	
	3	15.4	5.9	
	7	17.9	6.8	
	14	31.4	11.2	
	28	50.0	18.5	
SG/35SX	1	1.9	0.4	6.89
	3	3.0	1.6	7.25
	7	4.9	2.6	8.82
	14	7.2	4.4	8.95
SG/40SX	1	1.6	0.3	8.15
	3	3.3	1.5	8.81
	7	4.7	2.7	8.91
	14	8.4	5.0	9.00
SG/45SX	1	1.1	0.2	7.52
	3	1.8	0.8	7.62
	7	3.7	1.1	8.05
	14	5.5	2.1	8.52
	28	6.8	2.9	8.59

the increase was not strong enough to affect the glass matrix dissolution rate significantly. Fig. 11 shows the results for the release of Na^+ from all glass samples in a plot of $\log(NL_{Na})$ versus $\log t$. The slopes of the curves are about 0.5, in agreement with a diffusion-controlled process. Glass matrix dissolution and ion exchange are parallel processes. Comparing the rates of Si (Fig. 10) and Na (Fig.11) after one day, shows as expected that diffusion (ion exchange) is faster than dissolution at very short periods of time.

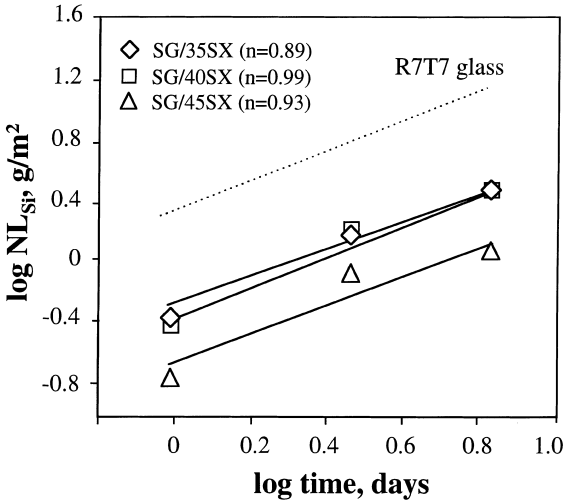

Fig. 10. Results of 7-day chemical durability tests (90°C, DI water). The data from Fig. 9 were plotted on log-scales. The slope identifies the kinetics of the process (glass matrix dissolution) and the intercept is the rate.

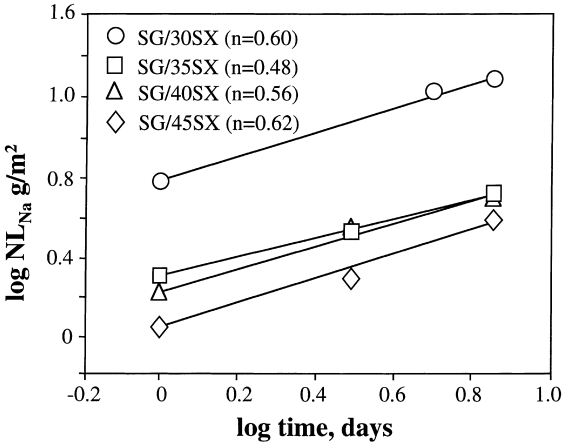

Fig. 11. Results of 7-day chemical durability tests (90°C, DI water). The normalized mass loss of Na as is plotted as a function of time (up to seven days) on log-scales (samples SG/30SX, SG/35SX, SG/40SX, and SG/45SX. The slope identifies the kinetics of the process (ion exchange) and the intercept is the rate.

Fig. 12 shows results of 28-day tests for the release of Si and Na. Samples SG/30SX and SG/45SX are compared. The data show, as in the previous figures, that the glass' chemical durability increases with increasing waste loading. The longer leaching time data for Na show that the rate decreased with time, consistent with a solid state diffusion process. The rate of matrix dissolution decreases because of silica saturation, consistent with glass dissolution models [1].

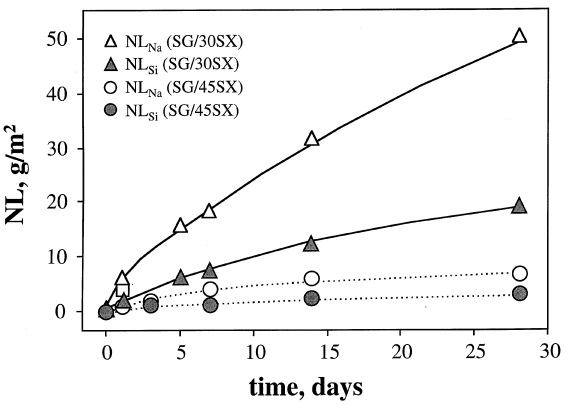

Fig. 12. Results of 28-day chemical durability tests (90°C, DI water). The normalized mass loss of Si and Na is plotted as a function of time for glass samples SG/30SX and SG/45SX.

4. Discussion

4.1. Microstructure of reaction sintered glasses

Glasses made with SX-type waste can be represented by the system Na_2O-X_mO_n-SiO_2($X_mO_n = Fe_2O_3 + Al_2O_3 + CeO_2$). These constituents make up 97 wt% of the final glass composition. The rest is essentially UO_2 and Cr_2O_3. UO_2 has been replaced by CeO_2. Al_2O_3, Cr_2O_3, and CeO_2 have exceeded their solubility limits in the glass and occur as pure crystalline oxide phases within the glass phase. Evidently, spinel phases did not form at the sintering temperature of 800°C. Spinel precipitation was extensively observed, however, when the waste containing spinel-forming components was melted into borosilicate glasses [3–6]. Iron and all minor constituents listed in Table 1 dissolved completely in the glass phase. The nano-scale and uniform size of eskolaite and ceria crystals suggests that their presence is a result of super-saturation of the developing glass phase rather than incomplete dissolution. The same observation was made with ZrO_2 [8,9]. It appears that this is an important mechanism of crystal formation in reaction sintered glasses. Rather than merely encapsulating or partially dissolving waste oxide phases in a glass phase [11], a glass ceramic-like waste form is obtained. The crystal number density is less homogeneous compared with high quality glass ceramics. One reason is that we are using fairly coarse silica particles. In the case of corundum, Al_2O_3, the evidence for a super-saturation/precipitation mechanism is less convincing. The corundum crystals (several microns in size) are much smaller than those of the starting materials (estimated size >10 μm). However, nano-size crystallites were not seen. Glass composition may be used as a criterion to support incomplete dissolution or precipitation. The radius of Al^{3+} is 0.057 nm and the ratio of the radii $r_{Al}:r_O = 0.43$. The Al^{3+} ion lies on the border between the coordination of 4 and 6. Thus, the molar ratio of $Na_2O:Al_2O_3$ in the glass determines whether Al^{3+} is a network modifier [AlO_6] or former [AlO_4]. If $Na_2O:Al_2O_3 < 1$ (peraluminous), two [AlO_4] tetrahedra will form per mole of Na_2O and the excess Al^{3+} forms [AlO_6] [16]. In our glasses $Na_2O:Al_2O_3 > 1$, independent of waste loading and Al^{3+} is a network former. One would expect that more aluminum could dissolve as network former than as a modifier before it reaches its solubility limit. This argument would support incomplete dissolution. In the following we discuss the super-saturation hypothesis in more detail.

Iron: The solubility of iron in silicate glasses is generally high and was not reached, even with the highest waste loading (45 wt% SX waste, corresponding to 6 wt% Fe_2O_3). Fe^{3+} is considered a glass former occupying tetrahedral sites [17–19]. Fe^{3+} forms primarily [FeO_4] tetrahedra in glasses and melts but Fe^{2+} is classified as modifier because of the smaller Fe–O bond valence, 0.50 v.u. [20]. Iron participated in spinel formation with other waste constituents (Cr, Ni, Mn, Al) upon glass melting at 1150°C [3–6] but did not at 800°C upon reaction sintering.

Chromium: Cr_2O_3 is isomorphous with corundum (Al_2O_3) and hematite (Fe_2O_3). However, Cr_2O_3 has a comparatively low solubility in silicate glasses due to its poor miscibility with SiO_2. Although the solubility of Cr_2O_3 increases with increasing alkali concentration, the maximum solubility in silicate glass is ~2 wt% [21]. In our sintered glasses with 13–17 wt% Na_2O, the solubility of Cr_2O_3 was ~0.7 wt% at 800°C. Li et al. [21] measured a solubility of 0.8 wt% in a borosilicate HLW glass (HTE-5612) melted at 1350°C. In borosilicate waste glasses, the prevailing valence of chromium is plus three. Cr^{3+} is octahedrally coordinated with six oxygen atoms independent of the oxidation state of chromium in the starting material [21].

Cerium: Rare-earth aluminosilicate glasses have received attention because they exhibit properties such as high glass transformation temperature, hardness, refractive indices, and chemical durability [22–24]. Cerium oxide disproportionates in the glass melt according to $4CeO_2 \leftrightarrow 2Ce_2O_3 + O_2$. For example, in a glass composed of $20CeO_2/25Al_2O_3/55SiO_2$ (mol%), melted at 1550°C in air, the ratio of Ce^{3+}:Ce^{4+} was 8:1 [25]. Our SX-type waste glasses were prepared at a much lower temperature (800°C). Hence, the ratio of Ce^{3+}/Ce^{4+} is expected to be much in favor of Ce^{4+}. This assumption is in agreement with the occurrence of ceria (Figs. 5–7). Ce^{4+}, Ce^{3+}, and other rare-earth element (REE) oxides act primarily as network modifiers indicated by an increase in non-bridging oxygen with increasing concentration of REE in the glass [23,26]. In rare-earth aluminosilicate glasses Ce^{4+} ions can balance the charge of octahedral $[AlO_6]^{3-}$ or tetrahedral $[AlO_4]^{1-}$ units or non-bridging oxygen [26]. Cerium could have an interesting effect on local charge and structure of the developing glass during reaction sintering. In the beginning, Na_2O reacts with SiO_2, a low-melting glass forms in the surface region of SiO_2 particles [9], and waste constituents such as CeO_2 dissolve in it. The solubility of high field-strength oxides in glasses increases with increasing alkali concentration, by a mechanism related to the peralkaline effect ((Na + K)/Al > 1) [20]. For our purposes, this effect can be illustrated using the following reaction:

$$2(\text{Si–O–Na})_{\text{glass}} + (\text{M–O–M})_{\text{cryst.}} = 2(\text{M–O–Na})_{\text{glass}} + (\text{Si–O–Si})_{\text{glass}}, \quad (1)$$

where *M* is a high field-strength ion. The dissolution of CeO_2 may be a special case because cerium ions act as a modifier. Reaction (2) may take place initially when the

viscosity of the glass is low, e.g., near the $75SiO_2/25Na_2O$ (mol%) eutectic:

$$(\text{Si–O–Si})_{\text{glass}} + (\text{Ce–O–Ce})_{\text{cryst.}} = 2(\text{Si–O–Ce})_{\text{glass}}. \quad (2)$$

As the reaction proceeds, the concentration of Na^+ decreases because it diffuses further into the SiO_2 particles and supply from the waste will cease eventually. As Ce^{4+} is more efficient in charge balancing than Na^+, a decrease in Na_2O up to 15 mol% can be balanced by the dissolved Ce^{4+}. However, migration of Na^+ from the surface region of a silica particle into the interior results in super-saturation of ceria in the surface. The same happens to other oxides, whose solubility depends on Na_2O concentration in the glass. They will nucleate and precipitate eventually. However, crystal growth will be small because of slow diffusive kinetics at 800°C and high viscosity of the glass.

4.2. Mechanism of reaction sintering

The mechanism of glass formation by reaction sintering was briefly discussed in preceding studies [8,9]. As mentioned in Section 4.1, Na_2O is expected to initiate glass formation with amorphous silica particles:

$$(\text{Si–O–Si})_{\text{glass}} + (\text{Na–O–Na})_{\text{cryst.}} = 2(\text{Si–O–Na})_{\text{glass}}. \quad (3)$$

Reaction of alkalis with pure silica glass reduces the activation energy of diffusive transport until the molar percent of alkalis oxide reaches about 20 mol% [27]. This means that reaction of Na_2O with amorphous silica is increasingly vigorous in the beginning. The liquidus temperature of the binary system decreases to the applied temperature of 800°C, if the Na concentration reaches 25 mol%, the first eutectic with a temperature of 790°C [28]. Since reaction sintering is a surface-mediated process and the reacting volume is small initially, high Na concentrations are likely to be attained. Once the viscosity of the sodium silicate glass in the surface regions of silica particles is lowered enough, sintering, e.g., neck formation and growth takes place coupled with chemical reaction.

If half of the mass of SiO_2 forms a binary glass before Na_2O is significantly depleted in the waste and its supply to the glass phase ceases, then a molar ratio of $Na_2O{:}SiO_2$ of 1:3 is obtained and the liquidus temperature will be near 800°C. Applying principles of polymer theory, this binary glass is expected to contain 35% Q^4, 60% Q^3, and 5% Q^2 groups, where the Q^n notation refers to a silicon tetrahedron with n bridging oxygen. On average, each silicon tetrahedron has 0.7 non-bridging oxygen. Addition of Al_2O_3 to this glass would render Al^{3+} tetrahedrally coordinated, charge balanced by Na^+. This would result in a decrease in the number of non-bridging oxygen in the glass as shown by

$$2(\text{Si–O–Na})_{\text{glass}} + (\text{Al–O–Al})_{\text{cryst.}} = (\text{NaAl–O–Si–O–Al–O–SiNa})_{\text{glass}}. \quad (4)$$

Dissolution of Fe^{3+} may be similar to that of Al^{3+} [29,30]. We assume that all other waste components dissolve while the viscosity is low and that dissolution is faster than transport of Na into the unreacted fraction of the SiO_2 particles. Then the following transient glass composition is obtained: SiO_2 52.4, Na_2O 18.8, CaO 0.7, Fe_2O_3 6.8, Al_2O_3 12.1, Cr_2O_3 2.1, MnO_2 1.2, and CeO_2 6.0 (in wt% at 35 wt% waste loading).

Looking at pure ternary systems such as Na_2O–Fe_2O_3–SiO_2 and Na_2O–Al_2O_3–SiO_2 reveals that a low viscosity can be sustained by waste components such as Fe_2O_3 and Al_2O_3 as they dissolve in the sodium silicate glass. There are six eutectic compositions in the Na_2O–Fe_2O_3–SiO_2 system with temperatures between 750°C and 850°C with Fe_2O_3 up to 35 mol% [31]. The concentration of Fe_2O_3 in the eutectic compositions increases with increasing molar ratio of $Na_2O{:}SiO_2$. There are three eutectic compositions in the Na_2O–Al_2O_3–SiO_2 system with temperatures between 750°C and 850°C and with Al_2O_3 up to 10 mol% [32]. Apparently, Fe_2O_3 is more soluble than Al_2O_3 in the sodium–silicate glass.

Eventually, the concentration gradient of Na between the surface and the interior of a glass particle will disappear in favor of a chemically more homogeneous glass. The phases constituting the waste have been digested and previously isolated glass particles will sinter to form a continuous macroscopic glass phase. Homogeneity of the glass phase will depend on the total sintering time. Under our conditions, a fully homogenous glass was not obtained as indicated by the contrast between two glass phases (Figs. 2 and 3).

As depletion of Na mostly affects the surface region of former SiO_2 particles, it is not surprising that the crystalline phases, eskolaite and ceria crystallize preferentially in this region. The original phase boundaries (surfaces) of the largest SiO_2 particles are marked by the spherical arrangement of nano-size crystals. This pattern, together with the crystal size and the visibly narrow grain size distribution, gives strong evidence of a precipitation mechanism rather than incomplete dissolution.

The super-saturation of Cr_2O_3 is expected as it has extremely low solubility in glasses. However, the mechanism for super-saturation of Al_2O_3 and CeO_2 merits further consideration. According to the modified random-network (MRN) model [33], a glass consists of local regions of network former separated by 'channels' where non-bridging oxygen and network modifiers are connected. Network modifiers such as Na^+ ions diffuse faster by taking channels highly concentrated in non-bridging oxygen as easy pathways. In contrast, transport of network former is always slower (often by orders of magnitude) than those of network modifiers. Transport of network former, e.g., Al, in high-silica melt is closely

related to viscous flow [34]. Thus, a low transport rate is expected for Al_2O_3 toward the center of the SiO_2 particles where the concentration of Na is low and viscosity is high. Under these conditions Al_2O_3 remains relatively concentrated near the surface in the transient high Na glass. However, the absence of nano-size crystals indicates that its solubility has not yet been reached or there may be local super-saturation but corundum grows on undissolved crystals.

Ce^{4+} can act as charge compensator for $[AlO_4]$ and the cerium concentration may be high enough to stabilize aluminum in the glass network. As a network modifier Ce^{4+} is more strongly bonded to oxygen than alkali because of higher field-strengths. Therefore, cerium is less mobile than sodium and does not migrate toward the central regions of the SiO_2 particles. Rare-earth ions have been found to occur preferentially in clusters or in heterogeneous regions in silicate glasses [35,36]. Its relative concentration increases in the surface as Na becomes depleted. Finally, nucleation of ceria, a solid phase with a high melting point, takes place, leading to a high number density of clusters of nano-size crystals.

It is interesting that no precipitation of hematite (Fe_2O_3) was observed in SX glasses. Despite its higher solubility than Al_2O_3, The self-diffusion coefficient for Fe^{3+} is at least one order of magnitude higher than those for Ce^{3+} and Cr^{3+} in a borosilicate melt [37]. Thus, Fe^{3+} is more homogeneously distributed over a glass particle. Comparing melting temperatures, Fe_2O_3 (1570°C), Cr_2O_3 (1900°C), CeO_2 (1950°C), Al_2O_3 (2054°C), suggests that Fe_2O_3, being the oxide with the highest melting temperature, would have the least crystallization tendency in a glass or melt.

4.3. Short-term chemical durability

The beneficial effect of Al_2O_3 on chemical durability is well known [38] and relates directly to the structural role of the $[AlO_4]$ tetrahedron as a network former. In SX-type reaction sintered glasses aluminum is expected to have the same structural function.

The role of iron depends on its oxidation state (Fe^{3+}/Fe^{2+} ratio) which is determined by temperature and oxidation potential. We have not measured the Fe^{3+}/Fe^{2+} ratio. Therefore, iron will not be discussed.

Na_2O is commonly present in radioactive wastes and deteriorates the chemical durability of glasses, unless its modifier function is mitigated by elements such as aluminum. In SX glasses $Al_2O_3 + Fe_2O_3 + CeO_2$ ranges from 13 to 15 wt% and is expected to compensate the deleterious effect of Na_2O.

Although CeO_2 acts as network modifier, the Ce–O bond is much stronger than the Na–O bond. The field-strength for Na^+ at 298 K is 0.18 vs. 0.83 for Ce^{4+}. Therefore, CeO_2 will improve the chemical durability when replacing sodium in its function.

Microstructure can also affect the short-term chemical durability of a sintered glass. For example, SG/30SX has a forward rate of about 1 gm^{-2} d^{-1}. We examined SG/30SX under SEM and found that this glass was highly porous (~10 vol.%), compared with the other three glasses (1–3 vol.%). At low waste loading the concentration of Na_2O was too low for it to be an efficient sintering aid. Thus, reaction sintering may not have been complete to provide a low porosity glass within 3 h. Prolonged sintering of this glass in a hot isostatic press decreased porosity substantially and improved the glass' homogeneity and thus its chemical durability [39].

4.4. Long-term chemical durability

We searched for a suitable natural analogue for these silicate glasses. Based on chemical composition rhyolitic glasses (obsidians) and tektites are good matches (Table 4). Differences in compositions lie in the presence of CeO_2, the comparatively high alkali content and the lower aluminum content in the SX-type waste glass (Table 4). To quantify these differences, we calculated the free energy of hydration for the waste glass and the two natural glasses, using Paul's [40] method. Thermodynamic data for these calculations were published by Jantzen and Plodinec [41]. The results at 25°C are given in Table 4. The components in SX glasses, rhyolitic glasses and tektites with positive free energies of hydration, ΔG_{hydr}, are SiO_2, Al_2O_3, Fe_2O_3, and CeO_2. They improve chemical durability of the glass. The components with negative ΔG_{hydr}, e.g., Na_2O, K_2O, CaO, deteriorate chemical durability. As the ΔG_{hydr}-values are practically the same for all three glasses, we assume that the long-term durability of our waste glasses can be evaluated based on natural corrosion phenomena observed on rhyolites and tektite.

Table 4
Compositions of rhyolitic and sintered glasses and free energies of hydration

Elements	SX waste	Rhyolitic glass [9]	Tektite [41]
SiO_2	70.93	74.4	74.4
Al_2O_3	3.35	12.6	12.2
Fe_2O_3	6.24	2.2	5.58
Cr_2O_3	0.59	–	–
Na_2O	14.19	4.2	1.32
K_2O	–	4.0	2.61
CaO	0.90	1.3	1.52
MgO	–	0.3	1.85
MnO_2	1.00	–	0.11
CeO_2	2.80	–	–
TiO_2	–	–	0.76
ΔG^0_{hydr} (kJ/mol)	+2.3	+3.3	+3.6

Rhyolitic glasses have been studied extensively to extract information relevant to the evaluation of the long-term chemical durability of nuclear waste glasses [42–46]. Magonthier et al. [45] studied the natural corrosion of 52 000 yr. old Icelandic obsidian. Their results show that the corrosion rate was about 1.1 μm/1000 yr at $\leqslant 10$°C. Abdelouas [46] studied rhyolitic glasses naturally corroded in salt lakes in Bolivia and showed that secondary phases such as Sr-rich barite, cerianite, and Mg-rich smectite formed on the obsidians. These are similar in structure and composition to those observed on the French reference nuclear waste glass R7T7, corroded in saline solutions in the laboratory. The glass corrosion rate of a 30 000 years old sample was estimated to be 0.045 μm/1000 yr at 10°C [46]. The rates derived from observations on natural glasses should not be used as quantitative information for the waste glasses. However, rates in the range of 0.1–10 μm/1000 yr indicate that radioactive Cs and Sr will decay into their stable daughters within the waste form without any significant release due to corrosion. Technetium and plutonium are present in small concentrations in SX-type waste. Even they will mostly transmute within the glass prior to release.

5. Conclusions

Vitrification of radioactive waste by reaction sintering under pressure is an attractive alternative process to melting, particularly for radioactive wastes containing a lot of refractory oxides such a Cr_2O_3, Fe_2O_3, Al_2O_3, etc. Reaction sintering takes place at temperatures considerably (350°C) lower than melting. Amorphous silica is the only additive needed to make these glasses. Formation of spinel phases that limit the life-time of melters does not take place. Waste loading is higher and is limited only by product properties, i.e., lack of glass formation or chemical durability, not by processing parameters such as melter corrosion, volatility, drainage problems etc. Reaction sintered glasses with a loading of SX-type Hanford tank waste as high as 45 wt% were prepared within three hours at 800°C and a pressure of 28 MPa. Waste constituents such as Na_2O, CaO, MnO_2, and Fe_2O_3 dissolved homogeneously in the glass phase. Other oxides were either incompletely dissolved (Al_2O_3, 45%) or first completely dissolved and then partially precipitated (CeO_2, 25%; Cr_2O_3, 50%) from a supersaturated glass phase. This phenomenon could be explained in terms of the time-dependent Na concentration of the developing glass phase. The high silica content determines that our reaction-sintered glasses are intrinsically of high chemical durability. The deleterious effect of Na_2O on chemical durability is mitigated by the beneficial effect of Fe_2O_3, Al_2O_3, and CeO_2. Long-term chemical durability of the sintered glasses is expected to be high because the free energy of hydration is comparable to that of obsidians and tektites.

Acknowledgements

Analytical and scanning electron microscopy work was conducted at the Microbeam Analytical Facility in the Department of Earth and Planetary Sciences of the University of New Mexico. The facility is partially supported by NSF, NASA, and the State of New Mexico. We thank Dr A. Abdelouas for discussion of obsidian glasses and chemical durability.

References

[1] W. Lutze, in: W. Lutze, R.C. Ewing (Eds.), Radioactive Waste Form for the Future, North-Holland, New York, 1988, pp. 1–161.
[2] The Hanford Site Tank Waste Remediation System: An Update, Westinghouse Hanford, REPORT # WHC-SA-2124, 1996.
[3] P. Hrma, R.J. Robertus, Ceram. Eng. Sci. Proc. 14 (1993) 187.
[4] P. Hrma, Ceram. Trans. 45 (1994) 391.
[5] P. Hrma, G.F. Piepel, P.E. Redgate, D.E. Smith, M.J. Schweiger, Ceram. Trans. 61 (1995) 505.
[6] P. Hrma, J.D. Vienna, M.J. Schweiger, Ceram. Trans. 72 (1996) 449.
[7] Q. Rao, G.F. Piepel, P. Hrma, J.V. Crum, J. Non-Cryst. 220 (1997) 17.
[8] W. Lutze, W. Gong, A. Abdelouas, R.C Ewing, Mat. Res. Soc. Symp. Proc. 506 (1998) 223.
[9] W.L. Gong, W. Lutze, A. Abdelouas, R.C. Ewing, J. Nucl. Mater. 265 (1999) 12.
[10] R. Terai, M. Kinoshita, K. Eguchi, Osaka Kogyo Gijutsu Shikenjo Kiho 29 (1978) 36.
[11] S. Gahlert, G. Ondracek, in: W. Lutze, R.C. Ewing, Radioactive Waste Form for the Future, North-Holland, New York, 1988, pp. 162–192.
[12] M.A. Audero, A.M. Bevilacqua, N.B.M. de Bernasconi, J. Nucl. Mater. 223 (1995) 151.
[13] A.M. Bevilacqua, N.B.M. de Bernasconi, D.O. Russo, M.A. Audero, M.E. Sterba, A.D. Heredia, J. Nucl. Mater. 229 (1996) 187.
[14] W.L. Gong, A. Abdelouas, W. Lutze, to be published.
[15] DOE MCC-1 Static Leach Test Method, Nuclear Waste Materials Handbook, DOE/TIC-11400, 1982.
[16] H. Scholze, Glass Nature Structure and Properties, Springer, New York, 1990, pp. 135–137.
[17] G.E. Brown, K.D. Keefer, P.M. Fenn, Abstr. Prog. Geol. Soc. Amer. Ann. Mtg. 10 (1978) 373.
[18] G. Calas, J. Petiau, Bull. Mineral. 106 (1983) 33.
[19] T. Nishidam, J. Phys. Sci. A51 (1996) 620.
[20] P.C. Hess, in: J.F. Stebbins, P.F. McMillan, D.B. Dingwell (Eds.), Reviews in Mineralogy, vol. 32, Mineralogical Society of America, Washington, DC, 1995, pp. 145–189.
[21] H. Li, M.H. Langowski, P.R. Hrma, M.J. Schweiger, J.D. Vienna, D.E. Smith, Minor component study for simulated

high-level nuclear waste glasses, Report PNNL-10996 Washington, Richland, 1996.
[22] J.T. Kohli, J.E. Shelby, Phys. Chem. Glasses 32 (1991) 67.
[23] J.E. Shelby, Key Engin. Mater. 94/9 (1994) 43.
[24] S.L. Lin, C.S. Hwang, J. Non-Cryst. Solids 202 (1996) 61.
[25] A. Makishima, T. Shimohria, J. Non-Cryst. Solids 38&39 (1980) 661.
[26] S.L. Lin, C.S. Hwang, J.F. Lee, J. Mater. Res. 11 (1996) 2641.
[27] G.H. Frischat, Ionic Diffusion in Oxide Glasses, Trans. Tech. Publications, Aedermannsdorf, Switzerland, 1975.
[28] F.C. Kracek, J. Phys. Chem. 34 (1930) 1583.
[29] M.P. Dickson, P.C. Hess, Contrib. Miner. Petrol. 78 (1981) 352.
[30] M.P. Dickson, P.C. Hess, Contrib. Miner. Petrol. 92 (1986) 207.
[31] N.L. Bowen, J.F. Schairer, H.W.V. Williams, Amer. J. Sci. 5th Ser. 20 (1930) 421.
[32] E.F. Osborn, A. Muan, Phase Equilibrium Diagrams of Oxide Systems, Plate 4, published by American Ceramic Society and the Edward Orton Jr. Ceramic Foundation, 1960.
[33] G.N. Greaves, S.J. Gurman, C.R.A. Catlow, A.V. Chadwick, S. Houde-Walter, C.M.B. Henderson, B.R. Dobson, Phil. Mag. A 64 (1991) 1059.
[34] D.R. Baker, Geochim. Cosmochim. Acta 56 (1992) 617.
[35] G. Darab, H. Li, J.D. Vienna, J. Non-Cryst. Solids 226 (1998) 162.
[36] S. Sen, J.F. Stebbins, J. Non-Cryst. Solids 188 (1995) 54.
[37] O. Claßuen, C. Rüssel, J. Non-Cryst. Solids 215 (1997) 68.
[38] B.M.J. Smets, T.P.A. Lommen, Phys. Chem. Glasses 23 (1982) 83.
[39] W.L. Gong, W. Lutze, to be published.
[40] A. Paul, J. Mater. Sci. 12 (1977) 2246.
[41] C.M. Jantzen, J.M. Plodinec, J. Non-Cryst. Solids 67 (1984) 207.
[42] R.A. Zielinski, Nucl. Tech. 51 (1980) 197.
[43] A.P. Dickin, Nature 294 (1981) 342.
[44] R.C. Ewing, J.C. Jercinovic, Mater. Res. Soc. Symp. Proc. 84 (1987) 67.
[45] M.-C. Magonthier, J.C. Petit, J.-C. Dran, Appl. Geochem. Suppl.(1) (1992) 83.
[46] A. Abdelouas, PhD thesis, University of Strasbourg, 1996.